Electronic Structure and Magnetic Properties of $Y_2Ti(\mu\text{-}X)_2TiY_2$ (X, Y=H, F, Cl, Br) Isomers

Christine M. Aikens and Mark S. Gordon*

Department of Chemistry, Iowa State University, Ames, Iowa 50011

Received: June 28, 2002; In Final Form: October 25, 2002

The electronic structure and magnetic properties of homodinuclear titanium(III) molecules with halide and hydride ligands have been studied using single- and multireference methods. Natural orbital occupation numbers suggest that the singlet states are essentially diradical in character. Dynamic electron correlation is required for calculating quantitatively accurate energy gaps between the singlet and triplet states. Isotropic interaction parameters are calculated, and three of the compounds studied are predicted to be ferromagnetic at the MRMP2/TZV(p) level of theory. Zero-field splitting parameters are determined using CASSCF and MCQDPT spin−orbit coupling with three different electron operator methods. Timings for these methods are compared. Calculated dimerization energies suggest that all dimers studied are lower in energy than the corresponding monomers. Monomer structures and vibrational frequencies are reported.

1. Introduction

It has been noted that "the most important developments in molecular magnetism in the last two decades have concerned compounds where several magnetic centers interact" (ref 1, p 103). Two of the greatest challenges include the synthesis of molecular ferromagnets that retain their ferromagneticity at very high temperatures and the design of systems with strong interactions between distant metal centers.[2] Since the bonding and magnetic properties of homodinuclear molecules arise from complex interactions between the two metal centers and between the metal centers and the bridging and terminal ligands, it is important to understand how changes in the ligands affect the magnetic properties of the system. To this end, homodinuclear copper(II) d^9 molecules have been extensively studied, as they provide a molecular system with one unpaired electron on each metal atom.[1−17] Homodinuclear titanium(III) molecules also have one unpaired electron on each metal center and provide an essential contrast to the copper(II) d^9 molecules because of differences in orbital occupation for the unpaired electrons and the greater radial extension of the Ti d orbitals.

Compounds containing titanium have long been studied for their interesting magnetic properties.[18−23] Recently, linear oxo-bridged heterodinuclear and homodinuclear compounds of titanium(III) have been examined using electron paramagnetic resonance (EPR), magnetic susceptibility, and ab initio calculations, and some compounds have been found to be ferromagnetic.[24−26] Two possible explanations have been advanced for the origin of the Ti−Ti exchange interaction that is apparently responsible for the observed magnetic properties: the direct overlap of the occupied Ti d orbitals or an intramolecular superexchange pathway via the bridging ligands.[27] For an exchange pathway involving the direct overlap of d orbitals, a decrease in the metal−metal distance generally leads to an increase in the magnitude of the antiferromagnetic interaction.[28] In a system with sizable bridging ligands, the large Ti−Ti distance prevents the direct overlap of d orbitals and necessitates a superexchange pathway. Such pathways normally result in a smaller antiferromagnetic effect than does the direct overlap pathway.[28] A few of the oxo-bridged dinuclear compounds do not interact via a superexchange pathway and consequently have a very small metal−metal interaction.[24,29] Most of the dinuclear titanium(III) complexes studied to this point are antiferromagnetic,[27,28,30−38] although two dinuclear complexes with extended ligand systems are also reported to be weakly ferromagnetic.[34]

Many of the experimentally known dititanium(III) bridged compounds have a planar ring structure,[27,30−32,35−37] so the D_{2h} isomers of $Ti_2X_2Y_4$ of interest in this work may be viewed as models for these compounds. Previous computational research has emphasized Ti_2H_6 as the simplest prototype for homodinuclear titanium(III) systems.[39,40] In this work, we examine changes in magnetic properties and electronic structure due to variations in the bridging and terminal ligands in these systems, with X, Y = H, F, Cl, Br.

The dominant magnetic effect in most cases is the isotropic interaction. This is an electrostatic phenomenon that may be formally described as a coupling between local spin operators $\mathbf{S}_A$ and $\mathbf{S}_B$. The Hamiltonian for the coupling may be written

$$\mathscr{H} = -2J\mathbf{S_A}\cdot\mathbf{S_B}$$

The isotropic exchange interaction parameter is defined by

$$2J = E(S = 0) - E(S = 1)$$

where S is the spin quantum number for the system, and the magnetic susceptibility is given by

$$\chi = \frac{2Ng^2\beta^2}{kT}\left[3 + \exp\left(\frac{-2J}{kT}\right)\right]^{-1}$$

where N is Avogadro's number, g is the average electronic gyromagnetic ratio, β is the Bohr magneton, k is the Boltzmann constant, and T is the temperature. In molecules with two local doublets that interact through bridging ligands, the two local spin states S_A and S_B have singlet and triplet coupling. As long as the isotropic interaction is dominant, the total spin quantum

* Corresponding author. E-mail: mark@si.fi.ameslab.gov.

10.1021/jp021537x CCC: $25.00
Published on Web 12/06/2002

number S is a good quantum number.[1] If the singlet ($S = 0$) is the ground state ($J < 0$), then the interaction is antiferromagnetic; if the triplet ($S = 1$) is the ground state ($J > 0$), then the interaction is ferromagnetic. When the interaction is antiferromagnetic, the magnetic susceptibility goes through a maximum (the Néel temperature) as the temperature decreases. The temperature T_{max} at which this occurs is related to J by

$$|2J|/kT_{max} = 1.599$$

where $k = 0.695$ cm^{-1} K^{-1}. This relation may be used to compare experimentally observable susceptibility maxima with calculated isotropic interaction parameters.

If the isotropic interaction is small, then other magnetic properties such as the dipolar interaction and anisotropic interaction (also called the pseudodipolar interaction) may become important. This may have especially important effects on the magnetic properties of the system if the triplet state is the ground state. In a dinuclear complex such as D_{2h} $Ti_2X_2Y_4$, the interaction of the two local doublets leads to a zero-field splitting (ZFS) of the triplet state. The electron paramagnetic resonance (EPR) spectrum of the triplet state may be described by the Hamiltonian

$$\mathcal{H} = \beta S\cdot\mathbf{g}\cdot H + S\cdot\mathbf{D}\cdot S$$

where the first term accounts for the Zeeman perturbation due to the magnetic field H and the **g** tensor and the second term accounts for the dipolar and anisotropic interactions, where **D** is the ZFS tensor.[10] The zero-field splitting parameters are calculated from the principal values of **D** by[10]

$$D = 3D_z/2$$

$$E = (D_x - D_y)/2$$

where D is the axial splitting parameter and E is the nonaxial (rhombic) splitting parameter. The dipolar term is often the minor contribution to **D** and is often reasonably estimated from the point dipole approximation.[1] The anisotropic (pseudodipolar) exchange interaction results from the synergistic effects of the local spin−orbit coupling (SOC) perturbations and the exchange interaction between the ground state of one magnetic center with the excited states of the other.[1,35] In a symmetric dimer, the zero-field splitting parameters D and E are composed of the dipolar contributions D_d and E_d and the pseudodipolar contributions D_e and E_e according to[35]

$$D = D_d + D_e$$

$$E = E_d + E_e$$

When the rhombic exchange parameter $|E_e|$ is larger than the axial exchange parameter $|D_e|$, SOC effects are larger perpendicular to the Ti−Ti axis than along it.

2. Computational Details

A triple-ζ with polarization (14s11p6d/10s8p3d) basis set was adopted for titanium, consisting of Wachter's basis set[41] with two additional sets of p functions[42] and an additional set of diffuse d functions.[43] In this notation (A/B), A and B refer to the primitive and contracted basis sets, respectively. For hydrogen, Dunning's (5s1p/3s1p) basis set was used.[44] For fluorine, the triple-ζ (10s6p/5s3p) basis set of Dunning was employed;[45] for chlorine, the triple-ζ (12s9p/6s5p) basis set of McLean and Chandler was employed;[46] and for bromine, the triple-ζ (14s11p5d/9s6p2d) basis set of Binning and Curtiss was employed.[47] Collectively, this basis set is referred to as TZV-(p). All geometry optimizations were performed with this basis set.

To predict reasonable energy-related quantities, polarization functions were added to the TZV(p) basis set. The basis set referred to as TZVP(f) adds f functions to the titanium ($\alpha = 0.40$),[48] two sets of d polarization functions to the halides, and diffuse s and p functions to the halides as well. The 2d polarization and diffuse sp function exponents are the default values in GAMESS.[49] The basis set called TZVP(fg) retains the halide basis set from TZVP(f) and adds one set of f ($\alpha = 0.591$) and g ($\alpha = 0.390$) functions and a set of diffuse s ($\alpha = 0.035$), p ($\alpha = 0.239$), and d ($\alpha = 0.0207$) functions to the TZV(p) titanium basis. These exponents are optimized for correlated titanium atoms.[50]

For the singlet homodinuclear titanium(III) molecules, preliminary geometry optimizations were carried out at the RHF level of theory. After convergence, modified virtual orbitals (MVOs) were generated by removing six electrons in the usual manner.[51] The resulting orbitals were used as a starting point for a two-configuration self-consistent field (TCSCF) geometry optimization. For the doublet and triplet states, geometry optimizations were performed at the ROHF level of theory.

Stationary points were characterized by calculating and diagonalizing the energy second-derivative (Hessian) matrix. Unless otherwise stated, these stationary points have no imaginary frequencies, so they are minima on their respective potential energy surfaces.

Dynamic electron correlation effects were included by carrying out multireference second-order perturbation theory (MRMP2)[52] single-point energy calculations at the TCSCF singlet geometries and ROHF triplet geometries. These single-point energy calculations were repeated with the TZVP(f) and TZVP(fg) basis sets as a test of basis set convergence. To obtain reasonable energies for the doublet states, Z-averaged perturbation theory (ZAPT2)[53] and MRMP2(1,1) calculations were carried out at the ROHF geometries.

Excited-state calculations require fully optimized reaction space (FORS) multiconfigurational SCF (MCSCF) calculations[54] (also called CASSCF), in this case with an active space consisting of 2 electrons in 10 orbitals. Spin−orbit coupling effects (SOC) are determined in three ways: a one-electron spin−orbit coupling operator method (HSO1),[55] a partial two-electron and full one-electron method (P2E),[56] and the full Pauli−Breit operator method (HSO2).[56] Both the complete active space SCF (CASSCF−SOC) and multiconfiguration quasi-degenerate perturbation spin−orbit coupling (MCQDPT-SOC)[57] techniques are used with each of the three methods.

All calculations were made using the electronic structure code GAMESS.[49] Molecules and orbitals were visualized using MacMolPlot,[58] a graphical interface to GAMESS.

3. Results and Discussion

Electronic Structure and Energetics. As noted in the earlier work on Ti_2H_6, the ground-state minima are either triplets or they are singlets with a high degree of diradical character. The lowest-energy singlet and triplet states are ^1A_g and $^3B_{1u}$, respectively. The lowest-energy structures for $Ti_2F_2H_4$ are an exception to the general pattern and are discussed in the next section. The natural orbital analysis of the TCSCF/TZV(p) wave functions (Figure 1) shows that the lowest-energy singlets all have at least 0.87 electrons in the lowest virtual orbitals. This

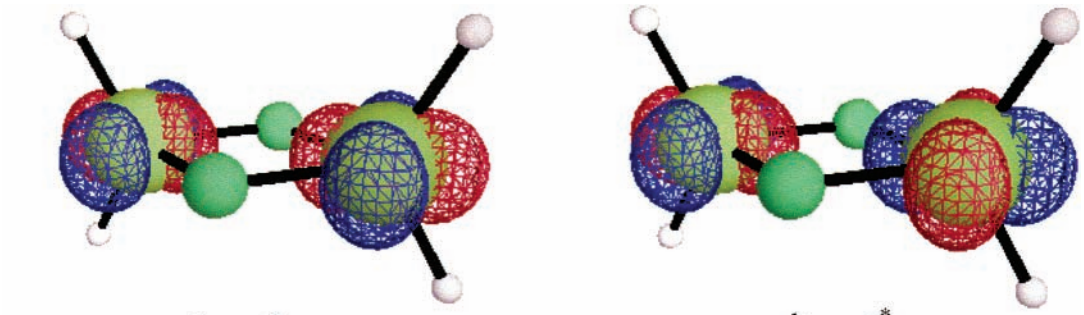

	a_g σ NOON	b_{1u} σ* NOON
$Ti_2H_2F_4$	1.13	0.87
$Ti_2H_2Cl_4$	1.11	0.89
$Ti_2H_2Br_4$	1.10	0.90
$Ti_2F_2H_4$	1.00	1.00
$Ti_2Cl_2H_4$	1.04	0.96
$Ti_2Br_2H_4$	1.05	0.95
Ti_2F_6	1.01	0.99
Ti_2Cl_6	1.03	0.97
Ti_2Br_6	1.05	0.95

Figure 1. Three-dimensional plots of the natural orbitals from a two-electron, two-orbital MCSCF/TZV(p) calculation. The orbital contour value for the plots is 0.06 bohr$^{3/2}$. The *z* axis is defined by the Ti−Ti axis. The orbitals shown are those for $Ti_2F_2H_4$. Natural orbital occupations numbers (NOONs) are shown below.

TABLE 1: Calculated Singlet−Triplet Energy Gap (*E*(triplet) − *E*(singlet)) in kcal/mol

	method/basis set for singlet−triplet calculation			
molecule	TCSCF/TZV(p)	MRMP2/TZV(p)	MRMP2/TZVP(f)	MRMP2/TZVP(fg)
Ti_2H_6[a]	0.56	1.33	1.40	1.43
Ti_2F_6	−0.12	−0.18	−0.23	−0.23
Ti_2Cl_6	−0.09	−0.01	0.27	0.90
Ti_2Br_6	−0.02	0.34	0.61	0.45
$Ti_2H_2F_4$	0.83	1.93	2.06	2.10
$Ti_2H_2Cl_4$	0.59	1.62	1.79	1.82
$Ti_2H_2Br_4$	0.52	1.53	1.68	1.70
$Ti_2F_2H_4$[b]	−0.11	−0.18	−0.20	−0.20
$Ti_2F_2H_4$[c]	0.12	0.24	0.28	0.28
$Ti_2F_2H_4$[d]	0.08	0.17	0.21	0.24
$Ti_2Cl_2H_4$	−0.04	0.06	0.34	0.34
$Ti_2Br_2H_4$	0.02	0.30	0.57	0.87

[a] Values from ref 39. [b] D_{2h} $^1A_g[(\sigma)(\sigma^*)]^{2/3}B_{1u}(\sigma,\sigma^*)$ state. [c] D_{2h} $^1A_g[(\delta)(\delta^*)]^{2/3}B_{1u}(\delta,\delta^*)$ state. [d] C_{2h} ^1A_u state.

suggests that these states are essentially singlet diradicals, probably with very small bonding interactions.

Dynamic electron correlation is required for calculating quantitatively accurate energy gaps between the singlet and triplet states (Table 1). At the TCSCF/TZV(p) level of theory, five of the triplet states are predicted to lie slightly (<0.2 kcal/mol) below the singlet states. However, inclusion of dynamic electron correlation via second-order perturbation theory lowers most of the singlet states preferentially. At the MRMP2/TZV-(p) level of theory, three of the triplet states lie below the corresponding singlet states. As the basis set size is increased, the singlet−triplet splitting increases by up to 0.3 kcal/mol on going from TZV(p) to TZVP(f) and by up to an additional 0.6 kcal/mol from TZVP(f) to TZVP(fg).

The lowest-energy singlet and triplet state geometries are shown in Table 2. Mulliken populations for the MCSCF and ROHF wave functions (Table 3) with the TZV(p) basis show positively charged titanium atoms, as expected with the anionic ligands. Charges on Ti range from +0.73 to +1.78, indicating highly polarized bonds. The Ti positive charges increase with the electronegativity of the ligands and with the number of electronegative ligands.

Although the orbitals for the $Ti_2X_2Y_4$ molecules are in principle able to form a direct Ti−Ti bond, there is apparently little such bonding based on the natural orbital occupation numbers (Figure 1). A similar conclusion was reached for singlet Ti_2H_6.

Lowest-Energy Structures for $Ti_2F_2H_4$. As for the other molecules in the series, the lowest-energy D_{2h} singlet state for $Ti_2F_2H_4$ is a ^1A_g state, while the lowest-energy triplet state is a $^3B_{1u}$ state. Two low-lying orbital configurations can contribute to these states. For the singlet, these are $[(\sigma)(\sigma^*)]^2$ and $[(\delta)(\delta^*)]^2$. For the other molecules in the series, the $[(\sigma)(\sigma^*)]^2$ configuration dominates the ground state, whereas $[(\delta)(\delta^*)]^2$ is an excited singlet state. However, the $[(\delta)(\delta^*)]^2$ configuration dominates the $Ti_2F_2H_4$ ground state, whereas the $[(\sigma)(\sigma^*)]^2$ configuration, at 0.9 kcal/mol, dominates the first excited singlet state at the TCSCF/TZV(p) level of theory. MCSCF(2,10) calculations show that there is essentially no mixing between the two configurations. The generalized valence bond perfect pairing (GVB-PP(1))[59] method (equivalent to TCSCF) was used to calculate the analytical Hessian for the two states, and both have two imaginary frequencies. Displacements along the imaginary modes lead to a common C_{2h} structure (Figure 3).

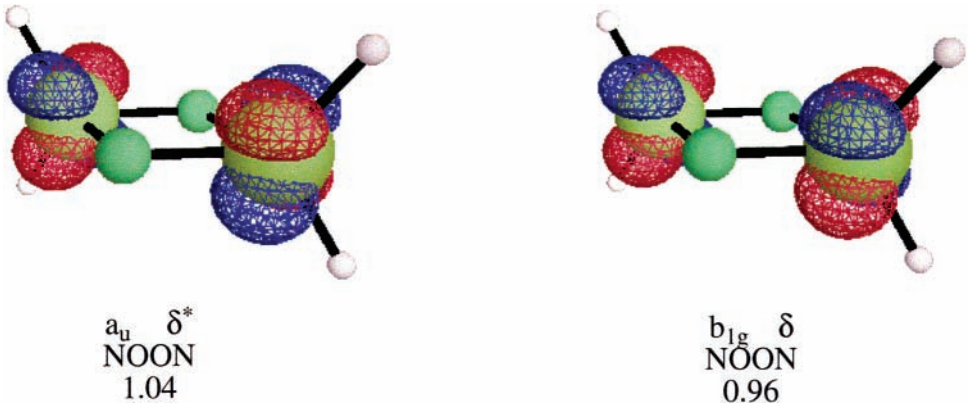

Figure 2. Three-dimensional plots of the natural orbitals for singlet $Ti_2F_2H_4$ from a two-electron, two-orbital MCSCF/TZV(p) calculation. The orbital contour value for the plots is 0.06 bohr$^{3/2}$. The *z* axis is defined by the Ti−Ti axis. Natural orbital occupation numbers (NOON) are shown.

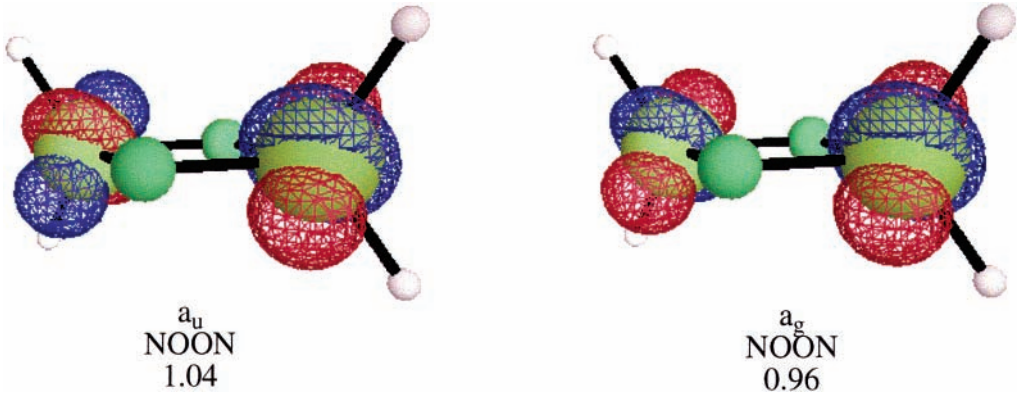

Figure 3. Three-dimensional plots of the natural orbitals for singlet $Ti_2F_2H_4$ with C_{2h} symmetry from a two-electron, two-orbital MCSCF/TZV(p) calculation. The orbital contour value for the plots is 0.06 bohr$^{3/2}$. The *z* axis is defined by the Ti−Ti axis. Natural orbital occupation numbers (NOON) are shown.

TABLE 2: Geometrical Parameters for the Lowest-Energy Singlet and Triplet States[a]

	distances (Å)				bond angles (deg)	
singlet states	Ti−Ti	Ti−X	Ti−Y	Y−Y	Y−Ti−Y	X−Ti−X
Ti_2F_6	3.249	2.020	1.814	3.289	130.1	72.9
Ti_2Cl_6	3.703	2.491	2.267	4.038	125.9	84.0
Ti_2Br_6	3.835	2.643	2.411	4.260	124.1	87.0
$Ti_2H_2F_4$	2.963	1.905	1.815	3.322	132.4	77.9
$Ti_2H_2Cl_4$	2.968	1.888	2.280	4.143	130.7	76.4
$Ti_2H_2Br_4$	2.975	1.887	2.425	4.388	129.6	75.9
$Ti_2F_2H_4$[b]	3.269	2.030	1.759	3.075	121.9	72.8
$Ti_2F_2H_4$[c]	3.279	2.029	1.745	2.853	109.7	72.1
$Ti_2F_2H_4$[d]	3.274	2.029	1.748	2.914	112.9	72.4
$Ti_2Cl_2H_4$	3.746	2.527	1.743	3.037	121.2	84.3
$Ti_2Br_2H_4$	3.876	2.684	1.741	3.032	121.0	87.5
triplet states						
Ti_2F_6	3.246	2.019	1.814	3.289	130.1	73.0
Ti_2Cl_6	3.712	2.491	2.268	4.039	125.9	83.7
Ti_2Br_6	3.853	2.644	2.412	4.264	124.2	86.5
$Ti_2H_2F_4$	2.989	1.909	1.815	3.317	132.1	77.0
$Ti_2H_2Cl_4$	2.987	1.892	2.280	4.136	130.2	75.7
$Ti_2H_2Br_4$	2.992	1.889	2.425	4.381	129.2	75.3
$Ti_2F_2H_4$[a]	3.268	2.030	1.759	3.075	121.9	72.8
$Ti_2F_2H_4$[b]	3.280	2.029	1.745	2.853	109.7	72.1
$Ti_2F_2H_4$[c]	3.274	2.029	1.749	2.922	113.3	72.4
$Ti_2Cl_2H_4$	3.758	2.527	1.743	3.038	121.3	83.9
$Ti_2Br_2H_4$	3.895	2.685	1.742	3.033	121.1	87.0

[a] X is the bridging ligand and Y is the terminal ligand in $Ti_2X_2Y_4$. [b] D_{2h} $^1A_g[(\sigma)(\sigma^*)]^{2/3}B_{1u}(\sigma,\sigma^*)$ state. [c] D_{2h} $^1A_g[(\delta)(\delta^*)]^{2/3}B_{1u}(\delta,\delta^*)$ state. [d] C_{2h} ^1A_u state.

This structure is 0.3 and 1.2 kcal/mol lower than the two D_{2h} states at the TCSCF/TZV(p) level of theory (Table 4). GVB-PP analytic Hessian calculations show that it is a minimum on the potential energy surface. Vibrational frequencies are reported in Table 5. The plane containing the Ti and F atoms makes an angle of 83.3° with the plane containing the Ti and H atoms. Other geometrical parameters are reported in Table 2.

TABLE 3: Mulliken Charges on Ti

molecule	singlet	triplet
Ti_2F_6	1.78	1.78
Ti_2Cl_6	0.93	0.94
Ti_2Br_6	0.75	0.75
$Ti_2H_2F_4$	1.46	1.46
$Ti_2H_2Cl_4$	0.89	0.89
$Ti_2H_2Br_4$	0.73	0.73
$Ti_2F_2H_4$[a]	1.12	1.12
$Ti_2F_2H_4$[b]	1.10	1.10
$Ti_2F_2H_4$[c]	1.11	1.11
$Ti_2Cl_2H_4$	0.85	0.85
$Ti_2Br_2H_4$	0.79	0.79

[a] D_{2h} $^1A_g[(\sigma)(\sigma^*)]^{2/3}B_{1u}(\sigma,\sigma^*)$ state. [b] D_{2h} $^1A_g[(\delta)(\delta^*)]^{2/3}B_{1u}(\delta,\delta^*)$ state. [c] C_{2h} ^1A_u state.

Monomer Structures and Vibrational Frequencies. A D_{3h} structure ($^2A_1'$ state) is found to be the lowest-energy minimum for the titanium trihalides, TiX_3. A C_{2v} structure ($^2A_1$ state) is found to be the lowest-energy minimum for both the TiX_2H and the $TiXH_2$ species. The C_{2v} state labels imply that *z* is the principal rotation axis and that the molecule lies in the *yz* plane. The ROHF/TZV(p) optimized geometries are given in Table 6.

In TiF_3, the calculated Ti−F distance of 1.819 Å is close to previously reported distances of 1.79,[60] 1.7978,[61] and 1.83[62] Å. The computed vibrational frequencies agree well with prior

TABLE 4: Relative Energies (kcal/mol) from the Lowest-Energy Singlet (C_{2h}) for Each Basis Set

	TCSCF/TZV(p)	MRMP2/TZV(p)	MRMP2/TZVP(f)	MRMP2/TZVP(fg)
$^1Ti_2F_2H_4$[a]	1.17	1.77	2.64	3.06
$^3Ti_2F_2H_4$[a]	1.05	1.59	2.44	2.86
$^1Ti_2F_2H_4$[b]	0.30	0.46	0.28	0.18
$^3Ti_2F_2H_4$[b]	0.41	0.70	0.55	0.47
$^1Ti_2F_2H_4$[c]	0.00	0.00	0.00	0.00
$^3Ti_2F_2H_4$[c]	0.08	0.17	0.21	0.24

[a] D_{2h} $^1A_g[(\sigma)(\sigma^*)]^2/^3B_{1u}(\sigma,\sigma^*)$ state. [b] D_{2h} $^1A_g[(\delta)(\delta^*)]^2/^3B_{1u}(\delta,\delta^*)$ state. [c] C_{2h} ^1A_u state.

TABLE 5: Theoretical Vibrational Frequencies (cm^{-1}) of $Ti_2X_2Y_4$ Molecules for the Lowest-Energy Singlet and Triplet States

mode	symmetry	activity	$^1Ti_2F_6$[a]	$^1Ti_2Cl_6$[a]	$^1Ti_2Br_6$[a]	$^1Ti_2H_2F_4$[a]	$^1Ti_2H_2Cl_4$[a]	$^1Ti_2H_2Br_4$[a]	$^1Ti_2F_2H_4$[b,e]	$^1Ti_2F_2H_4$[b,f]	$^1Ti_2F_2H_4$[b,g]	$^1Ti_2Cl_2H_4$[a]	$^1Ti_2Br_2H_4$[a]
Ti−Y stretching	a_g	Raman	700	432	334	689	432	362	1791	1796	1791	1814	1813
ring breathing	a_g	Raman	503	301	188	1369	1375	1369	484	492	490	294	218
bridge bending	a_g	Raman	302	171	116	289	240	172	255	276	267	150	111
Y−Ti−Y angle bending	a_g	Raman	126	70	44	118	70	44	658	641	536	657	653
bridge twisting	b_{1g}	Raman	148	89	54	580	508	481	948i	1207i	354	357	343
bridge stretching	b_{2g}	Raman	425	255	189	1284	1300	1304	411	325	341	240	175
Y−Ti−Y wagging	b_{2g}	Raman	160	108	78	162	115	104	399	429	427	369	356
Ti−Y stretching	b_{3g}	Raman	747	488	389	747	484	388	1690	1699	1698	1710	1711
Y−Ti−Y rocking	b_{3g}	Raman	90	69	50	85	48	35	279	230	245	284	291
Y−Ti−Y twisting	a_u	none	62	53	33	65	45	27	890i	1152i	278	350	341
Ti−Y stretching	b_{1u}	IR	671	407	309	660	380	266	1769	1773	1770	1799	1800
bridge stretching	b_{1u}	IR	528	297	187	1472	1488	1487	480	476	481	286	211
Y−Ti−Y bending	b_{1u}	IR	161	95	62	160	91	63	649	632	518	644	640
Ti−Y stretching	b_{2u}	IR	763	498	397	714	480	383	1704	1709	1710	1719	1717
bridge folding	b_{2u}	IR	247	132	83	827	762	747	119	113	115	80	61
Y−Ti−Y rocking	b_{2u}	IR	51	23	14	58	36	23	378	342	354	327	317
bridge stretching	b_{3u}	IR	439	317	253	1205	1205	1192	335	340	311	255	201
Y−Ti−Y wagging	b_{3u}	IR	131	83	55	139	87	71	493	481	462	425	409

mode	symmetry	activity	$^3Ti_2F_6$[c]	$^3Ti_2Cl_6$[c]	$^3Ti_2Br_6$[d]	$^3Ti_2H_2F_4$[c]	$^3Ti_2H_2Cl_4$[c]	$^3Ti_2H_2Br_4$[d]	$^3Ti_2F_2H_4$[c,e]	$^3Ti_2F_2H_4$[d,f]	$^3Ti_2F_2H_4$[c,g]	$^3Ti_2Cl_2H_4$[c]	$^3Ti_2Br_2H_4$[d]
Ti−Y stretching	a_g	Raman	700	431	335	689	434	367	1790	1797	1789	1811	1810
ring breathing	a_g	Raman	506	301	188	1370	1380	1374	487	492	490	294	218
bridge bending	a_g	Raman	306	178	121	295	244	174	258	277	265	156	116
Y−Ti−Y angle bending	a_g	Raman	125	69	44	120	69	43	659	641	526	660	658
bridge twisting	b_{1g}	Raman	146	84	52	570	496	467	674i	733i	355	258	284
bridge stretching	b_{2g}	Raman	425	255	188	1271	1288	1295	411	325	341	239	175
Y−Ti−Y wagging	b_{2g}	Raman	159	109	78	160	115	103	400	428	426	370	357
Ti−Y stretching	b_{3g}	Raman	747	489	389	744	483	386	1690	1699	1698	1714	1715
Y−Ti−Y rocking	b_{3g}	Raman	88	69	50	79	44	32	280	229	246	250	239
Y−Ti−Y twisting	a_u	none	62	42	27	62	33	22	672i	1987i	281	244	254
Ti−Y stretching	b_{1u}	IR	671	407	308	660	381	266	1769	1774	1769	1796	1796
bridge stretching	b_{1u}	IR	528	297	187	1466	1483	1484	481	476	477	285	210
Y−Ti−Y bending	b_{1u}	IR	160	95	62	160	89	63	649	632	508	646	643

TABLE 5 (Continued)

mode	symmetry	activity	$^3Ti_2F_6$[c]	$^3Ti_2Cl_6$[c]	$^3Ti_2Br_6$[d]	$^3Ti_2H_2F_4$[c]	$^3Ti_2H_2Cl_4$[c]	$^3Ti_2H_2Br_4$[d]	$^3Ti_2F_2H_4$[c,e]	$^3Ti_2F_2H_4$[d,f]	$^3Ti_2F_2H_4$[c,g]	$^3Ti_2Cl_2H_4$[c]	$^3Ti_2Br_2H_4$[d]
Ti−Y stretching	b_{2u}	IR	764	499	397	713	479	382	1703	1710	1709	1722	1721
bridge folding	b_{2u}	IR	247	132	83	829	766	751	120	110	114	64	48
Y−Ti−Y rocking	b_{2u}	IR	49	21	13	54	30	18	378	341	356	299	251
bridge stretching	b_{3u}	IR	440	315	251	1183	1188	1180	336	340	316	254	200
Y−Ti−Y wagging	b_{3u}	IR	131	83	55	138	86	69	494	479	455	424	410

[a] Results from MCSCF numerical Hessian calculation with double differencing and projection. [b] Results from the GVB analytic Hessian calculation. [c] Results from the ROHF analytic Hessian calculation. [d] Results from the ROHF numerical Hessian calculation with double differencing and projection. [e] D_{2h} $^1A_g[(\sigma)(\sigma^*)]^2/^3B_{1u}(\sigma,\sigma^*)$ state. [f] D_{2h} $^1A_g[(\delta)(\delta^*)]^2/^3B_{1u}(\delta,\delta^*)$ state. [g] C_{2h} ^1A_u state.

TABLE 6: ROHF/TZV(p) Geometries for the Titanium Monomers

molecule	symmetry/state	Ti−X[a]	Ti−H[a]	X−Ti−X or H−Ti−H angle[b]
TiF_3	$D_{3h}/^2A_1'$	1.819		120.0
$TiHF_2$	$C_{2v}/^2A_1$	1.821	1.754	127.6
TiH_2F	$C_{2v}/^2A_1$	1.824	1.764	116.5
$TiCl_3$	$D_{3h}/^2A_1'$	2.272		120.0
$TiHCl_2$	$C_{2v}/^2A_1$	2.292	1.723	128.4
TiH_2Cl	$C_{2v}/^2A_1$	2.315	1.749	116.0
$TiBr_3$	$D_{3h}/^2A_1'$	2.414		120.0
$TiHBr_2$	$C_{2v}/^2A_1$	2.436	1.720	129.2
TiH_2Br	$C_{2v}/^2A_1$	2.461	1.748	116.0

[a] Bond distances in angstroms. [b] Bond angles in degrees.

TABLE 7: Theoretical and Experimental Vibrational Frequencies (cm^{-1}) of TiX_3 Molecules (D_{3h})

mode	sym stretch A_1'	out-of-plane A_2''	asym stretch E'	asym bend E'
molecule	ν_1	ν_2	ν_3	ν_4
TiF_3	639	142	738	164
	630[a]	150[a]	735[a]	160[a]
	643[b]		740.6[b,c]	
		140.6[e]		
	665[d]	146[d]	764[d]	172[d]
$TiCl_3$	355	101	484	97
	296(15)[a]	120(6)[a]	505[a]	95(5)[a]
	338(17)[a]	118(6)[a]	465(24)[a]	91(5)[a]
		110 ± 12[f]	505 ± 10[f]	135 ± 12[f]
	350 ± 30[g]	110 ± 15[g]	500 ± 10[g]	135 ± 15[g]
	320(30)[h]	129(20)[h]	498(16)[h]	107(7)[h]
$TiBr_3$	218	88	388	63
	230[a]	80[a]	355[a]	58[a]

[a] Estimated in ref 60. [b] Reference 63. [c] Reference 64. [d] Reference 61. [e] Reference 62. [f] Reference 71. [g] References 65 and 72. [h] Reference 65.

estimates, calculations, and matrix isolation studies (see Table 7). This data provides additional evidence that the ν_3 band originally assigned to TiF_2 belongs to TiF_3.[63,64] In addition, the weak ν_1 symmetric stretch initially assigned to TiF_2[63] appears to belong to TiF_3. The confusion seems to have occurred because TiF_3 both disproportionates and sublimes unchanged upon heating;[64] this results in a spectrum that contains bands due to both TiF_4 and TiF_3 rather than TiF_3 and TiF_2 as assigned.

For $TiCl_3$, the calculated Ti−Cl distance of 2.272 Å differs considerably (~0.1 Å) from previously obtained Ti−Cl distances of 2.183[65] and 2.178[60]Å. Much of the available vibrational frequency data for $TiCl_3$ is for the solid state.[66−70] The few gas-phase studies are summarized here. As seen in Table 7, the computed vibrational frequencies are similar to those found previously. ν_4 in this work is 38 cm^{-1} lower than ν_4 from ref 71 but is similar to that in refs 60 and 65. ν_1 is 5−59 cm^{-1} higher than previously reported values, whereas ν_2 and ν_3 are within ± 28 cm^{-1}. Since the errors are not systematic and the previously reported frequencies vary significantly, the calculated frequencies have not been scaled.

For $TiBr_3$, the metal−halide distance and vibrational frequencies have previously been estimated from the equilibrium structures, force fields, and vibrational frequencies of $TiCl_3$ and TiI_3.[60] The previously estimated distance of 2.34 Å is 0.07 Å lower than the calculated distance of 2.414 Å. The vibrational frequencies differ from the previously estimated frequencies by 12, 8, 23, and 15 cm^{-1} for $\nu_1-\nu_4$ (see Table 7).

Since the vibrational frequencies calculated for the titanium trihalides are in reasonable agreement with prior estimates, calculations, and matrix isolation studies, it is reasonable to assume a similar level of agreement for the predicted frequencies for the TiX_2H and $TiXH_2$ species (Table 8).

Of the TiX_2H and $TiXH_2$ species studied here, only calculations on $TiHF_2$ and $TiHCl_2$ have been reported in the literature to date. For $TiHF_2$, Zakharov et al. found a Ti−H distance of 1.703 Å and a Ti−F distance of 1.741 Å with a calculated F−Ti−F angle of 129.0° using a 3-21G* basis set at the Hartree−Fock level of theory.[73] Vibrational data was not reported, although the stationary point was confirmed by diagonalizing the Hessian.[73] Determining the ground state of this molecule is elusive. The occupation of a d_{x^2}[74] orbital by a single electron on Ti leads to a $^2A_1$ state, whereas the occupation

TABLE 8: Theoretical Vibrational Frequencies (cm^{-1}) of $TiHX_2$ and TiH_2X Molecules (C_{2v})

mode	Ti−H stretch	Ti−X stretch	X−Ti−X bend	Ti−F stretch	angle bend	out-of-plane
symmetry	a_1	a_1	a_1	b_1	b_1	b_2
$TiHF_2$	1646	647	163	755	519	89
$TiHCl_2$	1689	358	85	411	534	213
$TiHBr_2$	1683	240	62	348	489	248
mode	Ti−H stretch	Ti−X stretch	H−Ti−H bend	Ti−H stretch	angle bend	out-of-plane
symmetry	a_1	a_1	a_1	b_1	b_1	b_2
TiH_2F	1737	584	727	1684	375	293
TiH_2Cl	1759	396	611	1732	369	309
TiH_2Br	1716	298	610	1682	288	268

TABLE 9: ROHF/TZV(p) Geometries for the Different States of $TiHCl_2$

state	Ti−X	Ti−H	X−Ti−X angle	relative energy (kcal/mol)
$^2A_1$ (ground)	2.292	1.723	128.4	0.00
$^2B_1$	2.296	1.710	136.7	1.72
$^2A_2$	2.316	1.723	120.8	5.29
$^2B_2$	2.335	1.689	147.4	24.63
	2.32[a]	1.68[a]	147.8[a]	

[a] Values from ref 75.

TABLE 10: Energy of Dimerization (kcal/mol) Using the TZV(p) Basis

molecule	ΔE_{elec} (MRMP2)	ΔZPE (MCSCF)	$\Delta H_{dimerization}$ (MRMP2)
Ti_2F_6[a]	−42.3	1.5	−40.7
Ti_2Cl_6[a]	−33.7	0.9	−32.8
Ti_2Br_6	−33.3	0.6	−32.7
$Ti_2H_2F_4$	−45.7	4.1	−41.6
$Ti_2H_2Cl_4$	−34.3	3.2	−31.1
$Ti_2H_2Br_4$	−34.8	3.0	−31.8
$Ti_2F_2H_4$[b]	−53.9	2.2	−51.6
$Ti_2Cl_2H_4$	−54.0	2.2	−51.8
$Ti_2Br_2H_4$	−56.3	2.0	−54.3

[a] Calculations for the triplet state (lowest-energy state at the MRMP2/TZV(p) level of theory). [b] Calculations for the C_{2h} structure.

of a d_{xz} orbital leads to a $^2B_1$ state. At the ROHF/TZV(p) level, the C_{2v} $^2B_1$ state is 0.4 kcal/mol lower in energy than the C_{2v} $^2A_1$ state. At this level of theory, the $^2B_1$ state has a positive definite Hessian, but the $^2A_1$ state does not. At the ZAPT2/TZV(p)//ROHF/TZV(p) level of theory, the $^2A_1$ state is lower than the $^2B_1$ state by 1.2 kcal/mol. UHF/TZV(p) calculations predict that the $^2B_1$ state is 0.2 kcal/mol lower in energy than the $^2A_1$ state and that both are minima. However, at the UMP2/TZV(p) level of theory, the $^2A_1$ state is lower than the $^2B_1$ state by 1.0 kcal/mol. At this level of theory, the $^2A_1$ state has a positive definite Hessian, but the $^2B_1$ state does not. The imaginary frequencies from the ROHF/TZV(p) $^2A_1$ and UMP2/TZV(p) $^2B_1$ state are out-of-plane bending modes. Calculations made in C_s symmetry show that these states end up converging to the lowest-energy planar structures for the given level of theory.

For $TiHCl_2$, previous calculations using generalized valence bond methods and ECP basis sets predict a planar compound with a Ti−H distance of 1.68−1.70 Å, a Ti−Cl distance of 2.32−2.33 Å, and a Cl−Ti−Cl angle of 140−148°.[75,76] The electronic state was not reported. In contrast, the Cl−Ti−Cl angle calculated in this work is 128.4°. To determine the origin of this difference, the minimum-energy structures for the $^2A_2$, $^2B_1$, and $^2B_2$ states were calculated. The reported geometrical parameters in ref 75 agree well with our calculated geometry for the $^2B_2$ state, which is 24.6 kcal/mol higher in energy than the $^2A_1$ state at the ROHF level of theory and 27.4 kcal/mol higher at the ZAPT2//ROHF level of theory (see Table 9).

Vibrational Frequencies for Dimers. Vibrational frequencies for the Raman- and IR-active bands of the $Ti_2X_2Y_4$ molecules are listed in Table 5. Very little experimental data is available for these compounds. Hastie, Hauge, and Margrave report an IR band at 745.5 cm^{-1}, which they attribute to a polymeric species such as $(TiF_3)_2$.[63] Two of our calculated frequencies for D_{2h} $F_2Ti(\mu\text{-}F)_2TiF_2$ fall within a reasonable range of this band. For the triplet state, a peak at 747 cm^{-1} (745 cm^{-1} for the slightly higher energy singlet state) appears to be a likely candidate, but because of the symmetry of the vibration, it is a Raman-active peak and should not be IR-active. A different peak at 764 cm^{-1} (762 cm^{-1} for the singlet) is within 19 cm^{-1} of the reported IR band and should be IR-active. After correcting for matrix shift effects of up to 20 cm^{-1},[1,63] these values could be even closer.

Dimerization Energies. The calculated TiX_3, TiX_2H, and $TiXH_2$ dimerization energies are listed in Table 10. Sørlie and Øye report the presence of Ti_2Cl_6 in high-temperature absorption spectroscopy.[77] They suggest a distorted tetrahedral structure for Ti_2Cl_6 in which two deformed tetrahedra share one edge. This structure would imply either C_{2v} or D_{2h} symmetry. Sørlie and Øye found the enthalpy of dimerization to be in the range of −32.7 to −34.2 kcal/mol.[77] Previous experiments in other laboratories found the enthalpy of dimerization to be −31.9 kcal/mol[78] and −40.6 kcal/mol.[79] The former values agree well with our calculated energy of dimerization of −32.8 kcal/mol for the D_{2h} structure using second-order perturbation theory. In general, the D_{2h} structures of $Ti_2X_2Y_4$ are 32.7−54.4 kcal/mol lower in energy than their separated monomers (see Table 10). Dimerization energies were calculated from the lowest-energy monomer structure to the lowest-energy dimer structure at the MRMP2/TZV(p) level of theory.

Previous theoretical calculations were made by Martinsky and Minot, who found a dimerization energy of −73.4 kcal/mol for their lowest-energy C_s Ti_2Cl_6 structure using density functional theory.[80] This is more than twice our predicted value. Their dibridged compound lies 3.1 kcal/mol above the C_s compound.[80] The dimer spin state was not specified.

Magnetic Properties. A. Isotropic Interaction. Magnetic properties of dinuclear complexes with a single unpaired electron on each magnetic center depend on the intramolecular interaction between the two metal centers. This interaction is affected by both the bridging ligands and the terminal ligands. As the bridging ligand changes from H to Br to Cl to F, the MRMP2/TZVP(fg) interaction becomes more ferromagnetic (J becomes

TABLE 11: $J(cm^{-1}) = E(singlet) - E(triplet)$

molecule	TCSCF/TZV(p)	MRMP2/TZV(p)	MRMP2/TZVP(f)	MRMP2/TZVP(fg)
Ti_2H_6	−98	−233	−246	−250
Ti_2F_6	20	32	40	41
Ti_2Cl_6	15	2	−47	−157
Ti_2Br_6	4	−59	−107	−78
$Ti_2H_2F_4$	−144	−337	−360	−367
$Ti_2H_2Cl_4$	−103	−283	−313	−318
$Ti_2H_2Br_4$	−90	−268	−294	−298
$Ti_2F_2H_4$[a]	20	32	35	35
$Ti_2F_2H_4$[b]	−20	−42	−49	−50
$Ti_2F_2H_4$[c]	−14	−30	−37	−41
$Ti_2Cl_2H_4$	7	−10	−59	−60
$Ti_2Br_2H_4$	−4	−52	−100	−153

[a] D_{2h} $^1A_g[(\sigma)(\sigma^*)]^{2/3}B_{1u}(\sigma,\sigma^*)$ state. [b] D_{2h} $^1A_g[(\delta)(\delta^*)]^{2/3}B_{1u}(\delta,\delta^*)$ state. [c] C_{2h} ^1A_u state.

less negative) (Table 11). As the terminal ligand changes from H to Br to Cl to F, the interaction becomes more antiferromagnetic (*J* becomes more negative). The isotropic interactions for the halide series range from 41 to -367 cm^{-1} at the MRMP2/TZVP(fg) level of theory. Note that dynamic correlation and larger basis sets have important effects on these predictions.

Experimentally observed *J* values for planar-ring Ti compounds fall within the range predicted by MRMP2 calculations. For example, for $((C_5H_5)_2TiCl)_2$ and $((C_5H_5)_2TiBr)_2$, observed *J* values are -70 to -85 cm^{-1} and -125 cm^{-1}, respectively, after adjusting for the difference in the isotropic interaction parameter definition.[32] These are similar to the corresponding values in Table 11. On the basis of a susceptibility maximum at 170 K, $((C_5H_5)_2TiCl)_2$ has an observed *J* value of -96 cm^{-1}.[30,31] Stucky et al. found *J* values of -111, -160, and -138 cm^{-1} for $((C_5H_5)_2TiCl)_2$, $((CH_3C_4H_5)_2TiCl)_2$, and $((CH_3C_4H_5)_2TiBr)_2$, respectively.[27] Although the halide terminal ligands may have isotropic interactions that are different from those of the organic terminal ligands, the predicted trend of increasing antiferromaticity for a given terminal ligand as the bridging ligand changes from chloride to bromide is consistent with the experiments.[27,32] Also of note is the observation that no susceptibility maximum for $((C_5H_5)_2TiF)_2$ was observed experimentally between 80 and 380 K.[32] The susceptibility maximum may be used experimentally to determine the antiferromagneticity of a compound. Since the theoretical calculations show that fluoride is a more ferromagnetic bridging ligand than chloride or bromide, this suggests either that the isotropic interaction for $((C_5H_5)_2TiF)_2$ is slightly antiferromagnetic with $0 > J > -44$ cm^{-1} (80 K) or that the interaction is ferromagnetic.

An interesting correlation may be noted between the natural orbital occupation numbers for a series of compounds and the ferromagneticity of these compounds by comparing Figure 1 and Table 11. As the diradical character of the compound becomes more pronounced and the NOON approaches 1, the ferromagneticity of the compound increases. This is consistent with the increase in the electronegativity of the bridging ligand.

B. Spin−Orbit Coupling Calculations. An initial state-averaged 2-electron, 10-orbital MCSCF calculation at the TCSCF/TZV(p) ^1A_g ground-state geometry was used to obtain a set of starting orbitals. Then, a second 2-electron, 10-orbital MCSCF calculation was carried out with no orbital symmetry constraints and with each of the first 20 singlet states weighted equally. Using this wave function as a starting point, a 2-electron, 10-orbital MCSCF calculation with the core and virtual orbitals frozen was run at the same geometry to obtain the first 20 triplet states. The singlet- and triplet-state orbitals were used in the CASSCF spin−orbit coupling (CASSCF-SOC) calculations. The orbitals from the 20 singlet-state calculation were used in the MCQDPT spin−orbit coupling (MCQDPT-SOC) calculations. The order and energies of the excited states vary slightly for the different $Ti_2X_2Y_4$ molecules but are qualitatively similar to those reported for Ti_2H_6.[40]

Inspection of the eigenvectors of the spin-mixed states allows for the identification of those adiabatic states that mix with the predominant state as well as that angular momentum operator that is responsible for the mixing. These adiabatic states and operators are exactly the same as those previously reported for Ti_2H_6, although the weightings vary slightly.[40] It is interesting to compare the performance of the three alternative methods for spin−orbit coupling calculations: the full two-electron (HSO2), partial two-electron (P2E), and one-electron method with effective nuclear charges (HSO1). Compared with HSO2, for CASSCF-SOC and MCQDPT-SOC, the coefficients in the eigenvectors of the spin states are within ± 0.00002 for P2E and ± 0.002 for HSO1. Except for $Ti_2F_2H_4$, the energy levels

TABLE 12: Spin−Orbit Coupling[a]

		CASSCF−SOC/TZV(p)			MCQDPT-SOC/TZV(p)		
molecule		HSO1	HSO2P	HSO2	HSO1	HSO2P	HSO2
Ti_2F_6	S_0	−7.491	−8.355	−8.355	−6.706	−7.589	−7.589
	$T_1 X$	−52.848	−53.697	−53.693	−45.358	−46.202	−46.198
	$T_1 Y$	−52.915	−53.771	−53.771	−45.415	−46.270	−46.269
	$T_1 Z$	−52.911	−53.766	−53.770	−45.430	−46.268	−46.271
	D_e	−0.030	−0.032	−0.038	−0.044	−0.032	−0.038
	E_e	0.034	0.037	0.039	0.029	0.034	0.035
Ti_2Cl_6	S_0	−8.927	−9.995	−9.995	−7.557	−8.686	−8.687
	$T_1 X$	−48.611	−49.658	−49.655	−37.103	−38.211	−38.208
	$T_1 Y$	−48.689	−49.745	−49.744	−37.159	−38.279	−38.278
	$T_1 Z$	−48.676	−49.731	−49.734	−37.147	−38.265	−38.268
	D_e	−0.026	−0.030	−0.035	−0.016	−0.020	−0.025
	E_e	0.039	0.043	0.044	0.028	0.034	0.035
Ti_2Br_6	S_0	−6.663	−7.774	−7.774	−5.460	−6.592	−6.592
	$T_1 X$	−18.562	−19.651	−19.649	19.473	18.350	18.352
	$T_1 Y$	−18.619	−19.718	−19.717	19.429	18.295	18.296
	$T_1 Z$	−18.607	−19.704	−19.707	19.439	18.307	18.305
	D_e	−0.016	−0.020	−0.024	−0.012	−0.016	−0.019
	E_e	0.028	0.034	0.034	0.022	0.027	0.028
$Ti_2H_2F_4$	S_0	−6.072	−6.622	−6.622	−5.872	−6.599	−6.599
	$T_1 X$	304.086	303.563	303.566	491.004	490.447	490.450
	$T_1 Y$	303.914	303.380	303.380	490.792	490.212	490.213
	$T_1 Z$	303.913	303.378	303.374	490.786	490.207	490.203
	D_e	−0.087	−0.094	−0.099	−0.112	−0.123	−0.129
	E_e	0.086	0.091	0.093	0.106	0.118	0.118
$Ti_2H_2Cl_4$	S_0	−7.709	−8.483	−8.484	−6.901	−7.881	−7.882
	$T_1 X$	215.218	214.450	214.457	446.386	445.533	445.538
	$T_1 Y$	215.044	214.261	214.266	446.154	445.265	445.268
	$T_1 Z$	215.045	214.262	214.257	446.133	445.242	445.237
	D_e	−0.086	−0.093	−0.104	−0.137	−0.157	−0.166
	E_{ee}	0.087	0.094	0.096	0.116	0.134	0.135
$Ti_2H_2Br_4$	S_0	−7.234	−8.042	−8.043	−6.706	−7.703	−7.704
	$T_1 X$	188.937	188.106	188.114	416.105	415.191	415.197
	$T_1 Y$	188.760	187.918	187.923	415.875	414.930	414.933
	$T_1 Z$	188.761	187.920	187.914	415.853	414.904	414.900
	D_e	−0.088	−0.092	−0.105	−0.137	−0.156	−0.165
	E_e	0.089	0.094	0.096	0.115	0.130	0.132
$Ti_2F_2H_4$[b]	S_0	−53.091	−56.216	−56.232	−98.661	−105.397	−105.420
	$T_1 X$	−91.490	−94.270	−94.226	−49.704	−57.300	−57.223
	$T_1 Y$	−91.567	−94.358	−94.317	−49.634	−57.142	−57.064
	$T_1 Z$	−90.612	−93.364	−93.381	−47.979	−55.561	−55.588
	D_e	0.916	0.950	0.890	1.690	1.660	1.556
	E_e	0.038	0.044	0.045	−0.035	−0.079	−0.079
$Ti_2F_2H_4$[c]	S_0	−28.829	−30.636	−30.644	−19.192	−21.147	−21.152
	$T_1 X$	11.685	9.742	9.772	58.295	56.227	56.246
	$T_1 Y$	11.683	9.740	9.768	58.253	56.125	56.145
	$T_1 Z$	12.205	10.289	10.278	58.494	56.433	56.426
	D_e	0.521	0.548	0.508	0.220	0.257	0.230
	E_e	0.001	0.001	0.002	0.021	0.051	0.050
$Ti_2F_2H_4$[d]	S_0	−29.488	−31.381	−31.39	−21.186	−23.351	−23.358
	$T_1 X$	2.680	0.668	0.697	59.049	56.375	56.396
	$T_1 Y$	2.672	0.659	0.686	59.285	56.839	56.861
	$T_1 Z$	3.213	1.227	1.215	59.418	56.767	56.758
	D_e	0.537	0.564	0.524	0.251	0.160	0.130
	E_e	0.004	0.005	0.005	−0.118	−0.232	−0.232
$Ti_2Cl_2H_4$	S_0	−12.999	−14.299	−14.299	−14.334	−16.292	−16.293
	$T_1 X$	−30.231	−31.506	−31.501	−36.987	−38.759	−38.753
	$T_1 Y$	−30.327	−31.615	−31.613	−37.076	−38.874	−38.871
	$T_1 Z$	−30.271	−31.556	−31.560	−36.953	−38.74	−38.745
	D_e	0.008	0.004	−0.003	0.078	0.076	0.067
	E_e	0.048	0.054	0.056	0.044	0.058	0.059
$Ti_2Br_2H_4$	S_0	−11.483	−12.813	−12.814	−12.727	−14.424	−14.425
	$T_1 X$	−0.004	−1.307	−1.303	5.237	3.569	3.573
	$T_1 Y$	−0.077	−1.397	−1.396	5.172	3.483	3.485
	$T_1 Z$	−0.019	−1.336	−1.340	5.308	3.626	3.622
	D_e	0.022	0.016	0.009	0.104	0.100	0.093
	E_e	0.037	0.045	0.047	0.033	0.043	0.044

[a] S_0, $T_1 X$, $T_1 Y$, and $T_1 Z$ are the energies (cm^{-1}) of the spin-mixed states for the lowest-energy singlet and *X*, *Y*, and *Z* components of the lowest-energy triplet state, respectively. D_e and E_e (cm^{-1}) are the axial and rhombic ZFS parameters, respectively. [b] D_{2h} $^1A_g[(\sigma)(\sigma^*)]^2/^3B_{1u}(\sigma,\sigma^*)$ state. [c] D_{2h} $^1A_g[(\delta)(\delta^*)]^2/^3B_{1u}(\delta,\delta^*)$ state. [d] C_{2h} ^1A_u state.

TABLE 13: CASSCF-SOC Timings[a]

molecule	method	total CPU time	spin−orbit coupling[c]	% total time	% SOC time[c]
Ti_2F_6	HSO1	229.6	56.4	1.58	0.39
	HSO2P	6355.8	6180.5	43.8	43.1
	HSO2	14514.2	14352.0	100.0	100.0
Ti_2Cl_6	HSO1	472.9	167.0	1.50	0.53
	HSO2P	10179.6	9871.1	32.2	31.5
	HSO2	31599.6	31304.0	100.0	100.0
Ti_2Br_6	HSO1	1780.0	1028.7	2.38	1.39
	HSO2P	35267.4	34429.9	47.1	46.4
	HSO2	74895.0	74137.5	100.0	100.0
Ti_2Br_6[b]	HSO1	531.5	256.6	3.22	1.58
	HSO2P	6621.7	6348.8	40.1	39.2
	HSO2	16492.6	16198.1	100.0	100.0
$Ti_2H_2F_4$	HSO1	178.2	37.2	2.33	0.49
	HSO2P	4292.3	4153.0	56.1	55.1
	HSO2	7656.3	7536.3	100.0	100.0
$Ti_2H_2Cl_4$	HSO1	270.4	81.2	1.91	0.58
	HSO2P	6052.6	5859.5	42.8	42.1
	HSO2	14141.1	13926.8	100.0	100.0
$Ti_2H_2Br_4$	HSO1	861.3	359.1	2.88	1.22
	HSO2P	17408.1	16962.5	58.2	57.5
	HSO2	29914.1	29515.7	100.0	100.0
$Ti_2F_2H_4$[d]	HSO1	108.1	21.6	1.89	0.38
	HSO2P	3043.9	2956.8	53.1	52.4
	HSO2	5728.6	5640.9	100.0	100.0
$Ti_2Cl_2H_4$	HSO1	147.8	34.5	1.66	0.39
	HSO2P	3617.5	3505.1	40.5	39.8
	HSO2	8921.2	8806.7	100.0	100.0
$Ti_2Br_2H_4$	HSO1	294.2	91.8	1.99	0.63
	HSO2P	6466.5	6265.6	43.7	42.9
	HSO2	14799.7	14598.1	100.0	100.0

[a] Timings for a 300-MHz UltraSPARC2 computer. [b] Timings for a 500-MHz AXP EV6 computer. [c] This category includes the time required for integral transformations and spin−orbit matrix element calculations. [d] D_{2h} $[(\sigma)(\sigma^*)]^2$ state.

TABLE 14: MCQDPT-SOC Timings[a]

molecule	method	total CPU time	spin−orbit coupling[b]	% total time	% SOC time[b]
Ti_2F_6	HSO1	3863.2	90.3	62.6	3.7
	HSO2P	5111.1	1500.7	82.8	62.2
	HSO2	6174.1	2412.8	100.0	100.0
Ti_2Cl_6	HSO1	9560.4	181.9	73.3	4.2
	HSO2P	11137.3	2471.3	85.4	56.5
	HSO2	13048.7	4374.7	100.0	100.0
Ti_2Br_6	HSO1	50172.1	800.1	81.7	7.1
	HSO2P	63878.7	6745.2	104.1	59.7
	HSO2	61380.2	11304.2	100.0	100.0
$Ti_2H_2F_4$	HSO1	2191.8	58.1	59.4	3.8
	HSO2P	3170.8	1022.4	85.9	67.3
	HSO2	3692.1	1519.2	100.0	100.0
$Ti_2H_2Cl_4$	HSO1	4471.8	105.3	68.4	4.6
	HSO2P	6022.4	1579.2	92.2	68.8
	HSO2	6533.6	2296.9	100.0	100.0
$Ti_2H_2Br_4$	HSO1	18638.0	363.9	81.0	6.4
	HSO2P	20682.6	3366.0	89.9	59.2
	HSO2	22996.9	5682.4	100.0	100.0
$Ti_2F_2H_4$[c]	HSO1	1620.4	42.7	60.2	3.9
	HSO2P	2320.5	711.9	86.1	65.5
	HSO2	2693.6	1086.2	100.0	100.0
$Ti_2Cl_2H_4$	HSO1	2103.7	56.5	62.8	4.3
	HSO2P	2908.5	859.7	86.8	65.8
	HSO2	3350.1	1307.2	100.0	100.0
$Ti_2Br_2H_4$	HSO1	4797.0	111.8	67.1	4.7
	HSO2P	6212.8	1538.0	86.9	64.4
	HSO2	7150.8	2388.1	100.0	100.0

[a] Timings for a 500-MHz AXP EV6 computer. [b] This category includes the time required for integral transformations and spin−orbit matrix element calculations. [c] D_{2h} $[(\sigma)(\sigma^*)]^2$ state.

calculated by P2E and HSO2 are practically the same and differ by no more than 0.008 cm^{-1}.

The principal axes *X*, *Y*, and *Z* for the T_1 (lowest triplet state) components can be determined from the coefficients of the eigenvectors. Then, the axial and rhombic pseudodipolar parameters D_e and E_e can be calculated as described previously.[40] These values are summarized in Table 12 for the six different methods used for determining spin−orbit coupling effects.

For the compounds with both bridging and terminal halide ligands, the spin-mixed triplet states are lower in energy than the lowest-energy singlet state for all calculations except Ti_2Br_6 MCQDPT-SOC. This mirrors the pattern in singlet−triplet splitting for the TCSCF/TZV(p) and MRMP2/TZV(p) calculations, as expected. For most of the calculations, the magnitude of E_e is slightly larger than the magnitude of D_e by up to 0.014 cm^{-1}. The one exception occurs for MCQDPT-SOC calculations on Ti_2F_6, for which $|D_e|$ is 0.015 cm^{-1} larger than $|E_e|$. In general, the magnitudes of D_e and E_e increase slightly as the method is improved from HSO1 to P2E to HSO2. For these compounds, the magnitudes of D_e and E_e decrease slightly as we go from CASSCF-SOC to MCQDPT-SOC calculations.

For the compounds with terminal halide ligands, all singlet states are lower in energy than the corresponding triplet states, as expected. In general, the magnitudes of D_e and E_e are similar. For the most part, $|D_e|$ is slightly larger than $|E_e|$ by up to 0.009 cm^{-1} for CASSCF-SOC or 0.031 cm^{-1} for MCQDPT-SOC. D_e becomes more negative and E_e becomes more positive for HSO2 relative to HSO1 and for MCQDPT-SOC relative to CASSCF-SOC.

For $Ti_2Cl_2H_4$ and $Ti_2Br_2H_4$, the magnitude of E_e is larger than the magnitude of D_e by up to 0.053 cm^{-1} for CASSCF-SOC calculations. However, this trend is reversed for MCQDPT-SOC calculations, for which $|D_e|$ is up to 0.071 cm^{-1} larger than $|E_e|$. D_e becomes more negative and E_e becomes more positive as the method improves from HSO1 to HSO2.

$Ti_2F_2H_4$ is the only compound that does not follow the general spin−orbit coupling patterns for $Ti_2X_2Y_4$ molecules. Its D_e values are an order of magnitude larger than other D_e values.

C. Spin−Orbit Coupling Timings. The relative times required for the various methods are given in Tables 13 and 14. Only timings for the σ,σ^* configuration of $Ti_2F_2H_4$ are included in the Tables since this structure is analogous to that of the other $Ti_2X_2Y_4$ molecules. In general, the CASSCF-SOC method requires less time than the MCQDPT-SOC method. For the CASSCF-SOC calculations, the P2E state energies are almost exactly the same as the HSO2 energies, but the method requires roughly 46% of the CPU time required for the HSO2 method on a Sun UltraSPARC2 300-MHz processor. This is approximately the same whether or not the setup time is included in the timings. For the MCQDPT-SOC calculations, the total time required for the P2E method is approximately 89% of the time required for the HSO2 method on a Compaq AXP EV6 500-MHz processor. However, the setup time for MCQDPT-SOC calculations is much greater than that for CASSCF-SOC calculations. If only the times for the spin−orbit coupling parts of the calculations are compared, then the P2E method requires only about 63% of the time required for the HSO2 method. For both CASSCF-SOC and MCQDPT-SOC calculations, the HSO1 method requires much less time than either the HSO2 or P2E method. As discussed in the previous section, the state energies vary slightly, but the D_e and E_e values calculated by the HSO1 method are close to those calculated by the other two methods. There is a slight accuracy tradeoff for a large computational time savings.

4. Conclusions

The compounds studied in this work have a high degree of diradical character. Dynamic electron correlation is required for calculating quantitatively accurate energy gaps between the singlet and triplet states. As the bridging ligand changes from H to Br to Cl to F, the interaction becomes more ferromagnetic; as the terminal ligand changes from H to Br to Cl to F, the interaction becomes more antiferromagnetic. Vibrational frequencies calculated for the monomers and dimers should help experimentalists determine whether these species are present in experiments. All dimers are predicted to be lower in energy than the corresponding separated monomers.

With the exception of $Ti_2F_2H_4$, spin−orbit coupling effects for these dinuclear titanium molecules are very similar to those for Ti_2H_6. Energies calculated by the HSO2 and P2E methods are virtually the same, even though the latter method requires significantly less computer time for CASSCF-SOC and MC-QDPT-SOC calculations.

Acknowledgment. C.M.A. thanks the National Science Foundation for a Predoctoral Fellowship. C.M.A. and M.S.G. also thank the National Science Foundation for providing a computer cluster to the Iowa State University Chemistry Department.

References and Notes

(1) Kahn, O. *Molecular Magnetism*; VCH: New York, 1993; Chapters 6−9.
(2) Kahn, O. *Angew. Chem., Int. Ed. Engl*. **1985**, *24*, 834.
(3) Hatfield, W. E. In *Magneto-Structural Correlations in Exchange Coupled Systems*; Willett, R. D., Gatteschi, D., Kahn, O. Eds.; NATO ASI Series; Reidel: Dordrecht, The Netherlands, 1985; pp 555−602.
(4) Rodríguez-Fortea, A.; Alemany, P.; Alvarez, S.; Ruiz, E. *Chem.−Eur. J*. **2001**, *7*, 627.
(5) Escuer, A.; Mautner, F. A.; Peñalba, E.; Vicente, R. *Inorg. Chem*. **1998**, *37*, 4190.
(6) Acevedo-Chávez, R.; Costas, M. E.; Escudero, R. *Inorg. Chem*. **1996**, *35*, 7430.
(7) Slangen, P. M.; van Koningsbruggen, P. J.; Goubitz, K.; Haasnoot, J. G.; Reedijk, J. *Inorg. Chem*. **1994**, *33*, 1121.
(8) Emori, S.; Todoko, K. *Bull. Chem. Soc. Jpn*. **1993**, *66*, 3513.
(9) Oshio, H.; Nagashima, U. *Inorg. Chem*. **1990**, *29*, 3321.
(10) Boillot, M.-L.; Journaux, Y.; Bencini, A.; Gatteschi, D.; Kahn, O. *Inorg. Chem*. **1985**, *24*, 263.
(11) Charlot, M. F.; Verdaguer, M.; Journaux, Y.; de Loth, P.; Daudey, J. P. *Inorg. Chem*. **1984**, *23*, 3802.
(12) Julve, M.; Verdaguer, M.; Gleizes, A.; Philoche-Levisalles, M.; Kahn, O. *Inorg. Chem*. **1984**, *23*, 3808.
(13) Charlot, M. F.; Jeannin, S.; Jeannin, Y.; Kahn, O.; Lucrece-Abaul, J.; Martin-Frere, J. *Inorg. Chem*. **1979**, *18*, 1675.
(14) Charlot, M. F.; Kahn, O.; Jeannin, S.; Jeannin, Y. *Inorg. Chem*. **1980**, *19*, 1411.
(15) Crawford, V. H.; Richardson, H. W.; Wasson, J. R.; Hodgson, D. J.; Hatfield, W. E. *Inorg. Chem*. **1976**, *15*, 2107.
(16) Solomon, E. I. In *Copper Proteins*; Spiro, T. G., Ed.; Wiley-Interscience: New York, 1981; Chapter 2.
(17) Calzado, C. J.; Cabrero, J.; Malrieu, J. P.; Caballol, R. *J. Chem. Phys*. **2002**, *116*, 2728.
(18) Fernandes, J. C.; Guimaraes, R. B.; Continentino, M. A.; Borges, H. A.; Valarelli, J. V.; Lacerda, A. *Phys. Rev. B* **1994**, *50*, 16754.
(19) Machin, D. J.; Murray, K. S.; Walton, R. A. *J. Chem. Soc. A* **1968**, *1*, 195.
(20) Fowles, G. W. A.; Lester, T. E.; Walton, R. A. *J. Chem. Soc. A* **1968**, *1*, 198.
(21) DeSavage, B. F.; Goff, J. F. *J. Appl. Phys*. **1967**, *38*, 1337.
(22) Strnat, K. J. *AIP Conf. Proc*. **1972**, *5*, 1047.
(23) Manjusri, G.; Mohan Babu, T. V. S. M.; Kaul, S. N.; Lucinski, T. *J. Phys.: Condens. Matter* **1997**, *9*, 2085.
(24) Lukens, W. W., Jr.; Andersen, R. A. *Inorg. Chem*. **1995**, *34*, 3440.
(25) (a) Fink, K.; Fink, R.; Staemmler, V. *Inorg. Chem*. **1994**, *33*, 6219. (b) Kolczewski, Ch.; Fink, K.; Staemmler, V. *Int. J. Quantum Chem*. **2000**, *76*, 137.
(26) Ren, Q.; Chen, Z.; Ren, J.; Wei, H.; Feng, W.; Zhang, L. *J. Phys. Chem. A* **2002**, *106*, 6161.
(27) Jungst, R.; Sekutowski, D.; Davis, J.; Luly, M.; Stucky, G. *Inorg. Chem*. **1977**, *16*, 1645.
(28) Fieselmann, B. F.; Hendrickson, D. N.; Stucky, G. D. *Inorg. Chem*. **1978**, *17*, 1841.
(29) Lukens, W. W., Jr.; Matsunaga, P. T.; Andersen, R. A. *Organometallics* **1998**, *17*, 5240.
(30) Martin, R. L.; Winter, G. *J. Chem. Soc*. **1965**, 4709.
(31) Canty, A. J.; Coutts, R. S. P.; Wailes, P. C. *Aust. J. Chem*. **1968**, *21*, 807.
(32) Coutts, R. S. P.; Wailes, P. C.; Martin, R. L. *J. Organomet. Chem*. **1973**, *47*, 375.
(33) (a) Fieselmann, B. F.; Stucky, G. D. *Inorg. Chem*. **1978**, *17*, 2074. (b) Fieselmann, B. F.; Hendrickson, D. N.; Stucky, G. D. *Inorg. Chem*. **1978**, *17*, 2078.
(34) Francesconi, L. C.; Corbin, D. R.; Hendrickson, D. N.; Stucky, G. D. *Inorg. Chem*. **1979**, *18*, 3074.
(35) Samuel, E.; Harrod, J. F.; Gourier, D.; Dromzee, Y.; Robert, F.; Jeannin, Y. *Inorg. Chem*. **1992**, *31*, 3252.
(36) Xin, S.; Harrod, J. F.; Samuel, E. *J. Am. Chem. Soc*. **1994**, *116*, 11562.
(37) Dick, D. G.; Stephan, D. W. *Can. J. Chem*. **1991**, *69*, 1146.
(38) Chen, L.; Cotton, F. A.; Dunbar, K. R.; Feng, X.; Heintz, R. A.; Uzelmeir, C. *Inorg. Chem*. **1996**, *35*, 7358.
(39) Webb, S. P.; Gordon, M. S. *J. Am. Chem. Soc*. **1998**, *120*, 3846.
(40) Webb, S. P.; Gordon, M. S. *J. Chem. Phys*. **1998**, *109*, 919.
(41) Wachters, A. J. H. *J. Chem. Phys*. **1970**, *52*, 1033.
(42) Hood, D. M.; Pitzer, R. M.; Schaefer, H. F., III. *J. Chem. Phys*. **1979**, *71*, 705.
(43) Rappe, A. K.; Smedley, T. A.; Goddard, W. A., III. *J. Phys. Chem*. **1981**, *85*, 2607.
(44) Dunning, T. H.; Hay, P. J. In *Methods of Electronic Structure Theory*; Schaefer H. F., III., Ed.; Plenum Press: New York. 1977; pp 1−27.
(45) Dunning, T. H. *J. Chem. Phys*. **1971**, *55*, 716.
(46) McLean, A. D.; Chandler, G. S. *J. Chem. Phys*. **1980**, *72*, 5639.
(47) (a) Binning, R. C.; Curtiss, L. A. *J. Comput. Chem*. **1990**, *11*, 1206. (b) Dunning, T. H., Jr. *J. Chem. Phys*. **1977**, *66*, 1382.
(48) Webb, S. P.; Gordon, M. S. *J. Am. Chem. Soc*. **1995**, *117*, 7197.
(49) Schmidt, M. W.; Baldridge, K. K.; Boatz, J. A.; Jensen, J. H.; Koseki, S.; Matsunaga, N.; Gordon, M. S.; Nguyen, K. A.; Su, S.; Windus, T. L.; Elbert, S. T.; Montgomery, J.; Dupuis, M. *J. Comput. Chem*. **1993**, *14*, 1347.
(50) Glezakou, V.-A.; Gordon, M. S. *J. Phys. Chem*. **1997**, *101*, 8714.
(51) Bauschlicher, C. W. *J. Chem. Phys*. **1980**, *72*, 880.
(52) (a) Hirao, K. *Chem. Phys. Lett*. **1992**, *190*, 374. (b) Hirao, K. *Chem. Phys. Lett*. **1992**, *196*, 397. (c) Hirao, K. *Int. J. Quantum Chem*. **1992**, *S26*, 517. (d) Hirao, K. *Chem. Phys. Lett*. **1993**, *201*, 59.
(53) (a) Jayatilaka, D.; Lee, T. J. *Chem. Phys. Lett*. **1992**, *199*, 211. (b) Lee, T. J.; Jayatilaka, D. *Chem. Phys. Lett*. **1993**, *201*, 1.
(54) (a) Sunberg, K. R.; Ruedenberg, K. In *Quantum Science*; Calais, J. L., Goscinski, O., Linderberg, J., Öhrn, Y., Eds.; Plenum Press: New York, 1976; p 505. (b) Cheung, L. M.; Sunberg, K. R.; Ruedenberg, K. *Int. J. Quantum Chem*. **1979**, *16*, 1103. (c) Ruedenberg, K.; Schmidt, M.; Gilbert, M. M.; Elbert, S. T. *Chem. Phys*. **1982**, *71*, 41. (d) Roos, B. O.; Taylor, P.; Siegbahn, P. E. M. *Chem. Phys*. **1980**, *48*, 157.
(55) Koseki, S.; Gordon, M. S.; Schmidt, M. W.; Matsunaga, N. *J. Phys. Chem*. **1995**, *99*, 12764.
(56) Fedorov, D. G.; Gordon, M. S. *J. Chem. Phys*. **2000**, *112*, 5611.
(57) Fedorov, D. G.; Finley, J. P. *Phys. Rev. A* **2001**, *64*, 042502.
(58) Bode, B. M.; Gordon, M. S. *J. Mol. Graphics Modell*. **1998**, *16*, 133.
(59) Hunt, W. J.; Hay, P. J.; Goddard, W. A. *J. Chem. Phys*. **1972**, *57*, 738.
(60) Giricheva, N. I.; Girichev, G. V.; Shlykov, S. A. *J. Struct. Chem*. **1991**, *32*, 602.
(61) Solomonik, V. G.; Sliznev, V. V.; Balabanov, N. B. *Russ. J. Inorg. Chem. (Engl. Transl.)* **1997**, *42*, 430.
(62) Yates, J. H.; Pitzer, R. M. *J. Chem. Phys*. **1979**, *70*, 4049.
(63) Hastie, J. W.; Hauge, R. H.; Margrave, J. L. *J. Chem. Phys*. **1969**, *51*, 2648.
(64) Beattie, I. R.; Jones, P. J.; Young, N. A. *Angew. Chem., Int. Ed. Engl*. **1989**, *28*, 313.
(65) Mamaeva, G. I.; Romanov, G. V.; Spiridonov, V. P.; Troyanov, S. I. *J. Struct. Chem*. **1987**, *28*, 846.
(66) Fraser, G. V.; Chalmers, J. M.; Charlton, V.; Cudby, M. E. A. *Solid State Commun*. **1977**, *21*, 933.
(67) Kanesaka, I.; Kawai, K.; Miyatake, T.; Kakugo, M. *Spectrochim. Acta, Part A* **1984**, *40*, 705.
(68) Kanesaka, I.; Yonezawa, M.; Kawai, K.; Miyatake, T.; Kakugo, M. *Spectrochim. Acta, Part A* **1986**, *42*, 1415.
(69) Miyaoka, H.; Hasebe, K.; Sawada, M.; Sano, H.; Mori, H.; Mizutani, G.; Ushioda, S.; Otsuka, N.; Terano, M. *Vib. Spectrosc*. **1998**, *17*, 183.

(70) Miyaoka, H.; Kuze, T.; Sano, H.; Mori, H.; Mizutani, G.; Ushioda, S.; Otsuka, N.; Terano, M. *J. Lumin.* **2000**, *87*−*89*, 709.

(71) Hastie, J. W.; Hauge, R. H.; Margrave, J. L. *High Temp. Sci*. **1971**, *3*, 257.

(72) Andersen, B.; Seip, H. M.; Strand, T. G.; Stolevik, R. *Acta Chem. Scand*. **1969**, *23*, 3224.

(73) Zakharov, I. I.; Zhidomirov, G. M.; Zakharov, V. A. *J. Mol. Catal*. **1991**, *68*, 149.

(74) This is referred to as d_{x^2} instead of d_{z^2} because of our chosen axis system.

(75) Bierwagen, E. P.; Bercaw, J. E.; Goddard, W. A., III. *J. Am. Chem. Soc*. **1994**, *116*, 1481.

(76) Steigerwald, M. L.; Goddard, W. A., III. *J. Am. Chem. Soc*. **1984**, *106*, 308.

(77) Sørlie, M.; Øye, H. A. *Inorg. Chem*. **1978**, *17*, 2473.

(78) Polyachenok, L. D.; Novikov, G. I.; Polyachenok, O. G. *Obshch. Prikl. Khim*. **1972**, 45.

(79) Sibbing, E.; Schäfer, H. *Z. Anorg. Allg. Chem*. **1974**, *410*, 67.

(80) Martinsky, C.; Minot, C. *Surf. Sci*. **2000**, *467*, 152.